We are IntechOpen, the world's leading publisher of Open Access books Built by scientists, for scientists

4,800
Open access books available

122,000
International authors and editors

135M
Downloads

Our authors are among the

154
Countries delivered to

TOP 1%
most cited scientists

12.2%
Contributors from top 500 universities

WEB OF SCIENCE™

Selection of our books indexed in the Book Citation Index in Web of Science™ Core Collection (BKCI)

Interested in publishing with us?
Contact book.department@intechopen.com

Numbers displayed above are based on latest data collected.
For more information visit www.intechopen.com

25

Compositional and Optical Gradient in Films of $PbZr_xTi_{1-x}O_3$ (PZT) Family

Ilze Aulika*
Center for Space Human Robotics, Italian Institute of Technology - IIT@PoliTO, Italy

1. Introduction

$Pb(Zr_xTi_{1-x})O_3$ (PZT) (x = 0-1) films have attracted the attention of researchers for the past 30 years due to their excellent ferroelectric (FE) and electromechanical properties, which have led to the commercialization of thin PZT films for ferroelectric random access memory (FeRAM), forming a market of several millions USD annually. Ferroelectricity of perovskite oxide thin films, especially PZT thin films, can be exploited in semiconductor devices to achieve non-volatile random access memory (NVRAM) with high-speed access and long endurance, which can overcome the barriers, encountered in current semiconductor memory technologies. The ferroelectricity can be also exploited to voltage dependent and thermally sensitive resistors, gas and humidity sensors. Besides, due to large pyroelectric coefficient of PZT, it has drawn interest for use in pyroelectric devices (Izyumskaya et al., 2007; Muralt, 2000; Whatmore et al., 2003).
PZT thin films have remarkable advantages over bulk materials:

- Can be directly deposited on platinized silicon to allow direct integration with electronics;
- Have superior electromechanical properties compared to other ferroelectric ceramics.

Thanks to that, PZT films have formed an integral part of the microelectromechanical systems (MEMS) in various applications such as sensors, actuated micromirrors for fine-tracking high-density optical data storage mechanisms (Yee et al., 2001), and tunable capacitors for high-frequency microwave applications, microelectromechanical systems, infrared detectors, applications in optical devices, for instance, rugate filters (Bovard, 1990), anti-reflection coatings (Oulette et al., 1991), and electro-optic modulators, to name a few.
Low density embedded FE memories are being considered for implementation not only in commercial devices, such as smart cards and cellular phones, but also for adaptive FE

*Alexandr Dejneka[2], Silvana Mergan[3], Marco Crepaldi[1], Lubomir Jastrabik[2], Qi Zhang[4], Andreja Benčan[5], Maria Kosec[5] and Vismants Zauls[6]
[1]*Center for Space Human Robotics, Italian Institute of Technology - IIT@PoliTO, Italy*
[2]*Institute of Physics, Academy of Science, Czech Republic*
[3]*HEARing CRC, University of Melbourn, Australia*
[4]*Cranfield University, School of Applied Sciences, United Kingdom*
[5]*"Jožef Stefan" Institute, Slovenia*
[6]*Institute of Solid State Physics, University of Latvia, Latvia*

memories in space applications. FE oxides have demonstrated high resistance to radioactivity (Philpy et al., 2003; Sternberg et al., 2003), what is important characteristic for space applications. Radiation test results on a prototype 1 kbit FE memory demonstrated that FE memory core using FE storage capacitors (Philpy et al., 2003), combined with hardened-by-design (HBD) CMOS circuitry, can attain high levels of tolerance to total ionizing dose and single event effects. Preliminary tests indicate that the hardness of the prototype memory exceeds 2 Mrads total ionizing dose and 163 MeV·cm²/mg linear energy transfer (LET) latch-up without the need for shielding (Kamp et al., 2004). FE memory can be designed to compete with any number of traditional semiconductor memory architectures, including SRAM, SDRAM, EEPROM and Flash memory (Kamp et al., 2004). This is accomplished by trading off internal write voltage with retention and endurance and taking advantage of the very fast read/write times of FE memory. FE memory can be designed to be exactly pin and function compatible with the other memory types. It follows that the memory types, which much softer to radiation exposure, can be replaced with FE memory without redesign of the circuit board (Kamp et al., 2004).

Every application of MEMS requires a different thickness and high quality of the functional film, leading to the challenge of manufacturing the film of the required thickness, epitaxy and purity. Among many methods for the fabrication of PZT thin films, chemical solution deposition (CSD), pulsed laser deposition (PLD), metal organic chemical vapor deposition (MOCVD), and physical vapor deposition such as RF sputtering have been widely employed. Among these techniques, chemical solution deposition methods like sol-gel processing offer low-capital costs, large-scale coating capabilities and easy control of chemical composition and homogeneity (Izyumskaya et al., 2007). However, the minimum thickness limitation of around 100 nm per layer for a crack-free and dense film deposited via CSD requires multiple coatings to reach the final thickness.

The broad applications of PZT films, and inter alia the growing interest in graded refractive index films for applications in optical devices (Xi et al., 2007; Wang et al., 2001), and applications in space environment, make it imperative to study the depth profile of composition and optical properties of thin films throughout a single layer and an entire coating. Moreover graded PZT thin films, e.g., with amplitude of ±20% at the 53/47 morphotropic phase boundary (MPB), have showed improved electrical performances (Ledermann et al., 2003), raising importance of depth profile analyses and control. Wherewith, information on the homogeneity of the films and the physical properties resulting from different processing methods represents crucial knowledge.

Gradients in optical properties (refractive index n, extinction coefficient k, abortion coefficient α, band gap etc) and chemical composition gradients have been reported, e.g., for sputtered PZT films (Deineka et al., 1999 and 2001; Vidyarthi et al., 2007; Chang et al., 2005) and for CSD-fabricated PZT films (Aulika et al., 2009; Calamea and Muralt, 2007; Etin et al., 2006; Impey et al., 1998; Ledermann et al., 2003; Marcus and Schwartz, 2000; Watts et al., 2005). Variation of chemical composition throughout the film thickness due to inhomogeneity results in variation of physical properties such as optical properties of the films, resistance to irradiation, and lowers or improves the performance of electromechanical systems. The understanding of the compositional gradient and physical properties resulting from different processing methods is crucial. Thus, the knowledge of the optical gradient within a film allows identification and further optimization of the thin film performance and applications in piezo- and ferro-devices.

2. Depth profile detection methods

A challenging aspect of homogeneity studies lies in the development of an appropriate characterization method, since the compositional variation must be determined on a small scale, within 100 nm. Depth profile detection methods can be divided into two categories:

- Destructive,
- Non-destructive methods.

The 1st category typically allows local visualization of thin films and element concentration analyses, what requires etching or cross section of the sample accompanied with spectroscopy methods. For visualization of the films well established microscopy techniques such as scanning electron microscopy (SEM), transmission electron microscopy (TEM), and atomic force microcopy (AFM) are widely used in the practice. For compositional analyses (qualitative and quantitative) energy-dispersive x-ray spectroscopy (EDXS, known also as EDX or EDS), photoelectron spectroscopy (XPS), secondary ion mass spectrometry (SIMS), Rutherford back scattering (RBS), electron energy loss spectroscopy (EELS) and other spectroscopies are applied. For example, the approach can be thought of simply as the analytical implementation of rf-sputter etching, where the atomized material is analyzed by its characteristic optical emission. This method is known as radiofrequency glow discharge atomic emission spectroscopy (rf-GD-AES) (Marcus and Schwartz, 2000): permits the depth-resolved elemental analysis of metallic, semiconducting, and insulating materials over depths of 20 nm–150 μm in a rapid fashion < 0.1–5 μm/min. The analytical data are reported as elemental emission intensities as a function of sputtering time, termed a qualitative depth profile. Qualitative depth profile can be also analyzed by the detection of concentration gradients of the chemical elements of PZT thin films using Z contrast TEM with EDX (Ledermann et al., 2003). In the work of Watts et al., 2005, the EDX was performed on $PbZr_{0.52}Ti_{0.48}O_3$ (PZT 52/48) thin films. Compositional profiles were determined along with analysis of the state of oxidation of the lead. The data were compared with bulk polycrystalline material as standard giving quantitative depth profile of the films.

Similar method to rf-GD-AES was presented in the work of Vidyarthi et al., 2007, where chemical composition and depth profiling of PZT films was investigated by glow discharge optical emission spectroscopy (GDOES). They used two samples, which chemical composition was measured by RBS, to calibrate GDOES for PZT quantitative compositional analysis.

SIMS was used to monitor the Pb, Zr, Ti, and C secondary ions in addition with the EDX to determine the oxidation state of the elements (Etin et al., 2006). Pb4*f*, Zr3*d*, and Ti2*p* and O1*s* spectra were used for calculation of film composition as a function of depth using calibration equations (Sugiyama et al., 2003 and 2004) presenting quantitative depth profile analyses.

Fascinating work have been done by Parish et al., 2008, where the use of multivariate statistical analysis (MSA) of EDS spectrum images (SIs) in scanning TEM (STEM) was extended to allow the two-dimensional (2D) quantitative analysis of cation segregation and depletion in PLZT thin films. STEM-EDS SIs method allows high-resolution (≤ 10 nm) quantification of cation distributions. Zr/Ti and La segregation are found to develop in a decidedly nonplanar fashion during crystallization, highlighting the need for 2D analysis.

The drawback for TEM and STEM-EDS SIs investigations is tedious and time-consuming sample preparation. Investigation using other methods such as RBS results in sample modification or even destruction after analysis. Also all other methods mentioned before

goes hand to hand with either sample distraction, compositional modification (e.g., impregnation of ions during milling with ion beam) or specific sample preparation needs. To conclude, examples given above for depth profile detection suffer from being ''local'', intrusive, destructive and unsuitable for real-time, inline monitoring of processes and surface/interface modifications of thin films.

What about the 2nd category: non-destructive methods of depth profile detection? In this category only sensitive, accurate, contactless optical techniques are giving this opportunity to analyze thin films in non-destructive way. Well know optical methods are, for example, reflectometry, interferometry and spectroscopic ellipsometry (SE). SE have several advantages regarding other optical methods eliminating such disadvantages as dependence on the intensity of the light source (reflectometry), vibrations and atmospheric disturbances (interferometry). SE is nondestructive, nonintrusive, and noninvasive, contactless optical technique, applied not only for the optical characterization of bulk materials and thin films, but also for in situ real-time measurement of multilayered film structures, interfaces, surfaces, and composites, during fabrication and processing.

SE has long been recognized as a powerful method for the characterization of thin films and their inhomogeneity. It has already been applied to refractive index depth profile studies of oxynitride SiO_2N_x films (Callard et al., 1998; Nguyen et al., 1996; Snyder et al., 1992; Rivory, 1998;) (additionally confirmed by chemical etching (Callard et al., 1998)), lead silicate glass (Trolier-McKinstry and Koh, 1998), oxidized copper layers (Nishizawa et al., 2004), polymers (Guenther et al., 2002), semiconductor indium tin oxide (ITO) films (Losurdo, 2004; Morton et al., 2002), sol-gel PZT thin films (Aulika et al, 2009) confirmed by TEM and EDX, and RF-sputtered self-polarized PZT thin films (Deineka et al., 2001), and was confirmed by discharge optical emission spectroscopy (GD-OES) and pyroelectric profile measurements by the laser intensity-modulation method (LIMM) (Deineka et al, January, 2001; Suchaneck et al., 2002). SE has also been applied to the study of ion implantation depth profiles in silicon wafers and confirmed by RBS (Boher et al., 1996; Fried et al, 2004). The sensitivity of SE was demonstrated on graded oxygen compositions in $YBa_2Cu_3O_{7-\delta}$ (YBCO) thin films, in which it was able to detect changes in the oxygen concentration to within one unit cell (Gibbons, and Trolier-McKinstry, 1999).

SE cannot quantitatively examine cation distribution at a length scale comparable with the feature sizes like in a case of STEM-EDS SIs method (Parish et al., 2008) since the measured area depends on the diameter of the incident light spot of SE (typically ~ 3 mm, by using focusing nuzzles it can be reduced till ~ 0.1 mm). As the result it is easy to perform relatively large area scans of the sample using SE, and evaluate information (for example, depth profile) in average across many features simultaneously. And thus SE studies gives an opportunity in non-destructive, rather fast and easy way to analyze the inhomogeneity of material and helps to understand how processing affects structure and thus properties in this system. Now more in details about this method.

2.1 Spectroscopic ellipsometry

Not very long time ago the development of spectroscopic ellipsometry made it possible to investigate the complex refractive index of thin films and bulks in a wide spectral range (gives access to fundamental physical parameters; morphology, crystal quality, chemical composition, or electrical conductivity), and detecting inhomogeneities of thin films, eliminating such disadvantages of other non-destructive and contactless optical technique as

dependence on the intensity of the light source (reflectometry), vibrations and atmospheric disturbances (interferometry) (Tompkins and Irene, NY 2005).
Typical ellipsometers can accurately measure ψ and Δ better than 0.01°. Due to such a high accuracy a change of the refractive index of 10^{-3} – 10^{-4}, and film thickness changes down to the sub-Å scale can easily be resolved with this technique (Tompkins and Irene, NY 2005). A reflectometer system can not accurately measure intensity values better than 0.1%, and therefore a reflectivity measurement is not sensitive enough for small changes of the material`s optical properties and for thin film thicknesses.
With spectral ellipsometry one can measure the dispersion of the complex dielectric constant of bulk materials and thin films with very high accuracy. This technique does not require a large size of the sample; it is enough to have a size of ~ 5×5 mm. In situ spectral ellipsometry studies allow detecting phase transition in thin films and surfaces (Dejneka et al., 2009), as well as of the interface what is very important for thin film and crystal studies.
For advanced optoelectronics and bandgap engineering applications is important to investigate the relationship between the microstructure, sample preparation conditions & optical properties. SE gives opportunity to detect technologically and scientifically important properties of thin films such as optical bang gap (Dejneka et al., 2010), thermo-optical properties (Aulika et al., 2007 and 2009; Dejneka et al., 2009), and optical gradient (Aulika et al., 2008 and 2009; Deineka et al., January, 2001).

2.2 What ellipsometry measures?

Ellipsometry measures the change of the polarization state of light upon reflection. It overcomes two major problems of conventional spectroscopy or reflectivity: the phase problem (in ellipsometry the phase is measured and does not have to be calculated by Kramers-Kronig relation) and the reference problem (ellipsometry requires relative, not absolute, intensities). Paul Drude was the first to study optical properties using the ellipsometry technique. He published the equation of ellipsometry in 1887, and his experimental results in 1888. Generally, after reflection on a sample the polarization state of the light is elliptical (Fig. 1). The electrical field components parallel and perpendicular, E_{ip} and E_{is}, with respect to the plane of incidence change their amplitude and phases due to reflection upon the sample. These total reflective coefficients are connected with the main ellipsometric angles ψ and Δ (Tompkins and Irene, NY 2005)

$$\tan\psi = \frac{|r_p|}{|r_s|} \quad \text{and} \quad tg\psi\, e^{i\Delta} = \frac{r_p}{r_s} = \frac{E_{ip}}{E_{is}} = \gamma\,,$$

where γ is the quantity of ellipticity, and $\Delta = \delta_p - \delta_s$ is the phase shift of the *p* and *s*-polarized light (Fig. 1). Reflection and transmittance coefficients can be found from Fresnel formulas, which on the other hand are containing information about the optical constants, thickness of the thin film (or thin films in the case of multilayer) incident angle of the light, and phase suspension of the light.
$\psi = \psi(\varepsilon, \sigma, \omega)$, and $\Delta = \Delta(\varepsilon, \sigma, \omega)$, where ε is the real part of dielectric function, σ is the real part of conductivity, and ω is the frequency. There are two equivalent descriptions: the first one operates with real and imaginary parts of the dielectric function ε_1, ε_2, the second one operates with the real part of the dielectric function and the real part of the conductivity. The ratio between conductivity and dielectric function $\sigma \propto \iota\omega\varepsilon$ makes these descriptions equivalent.

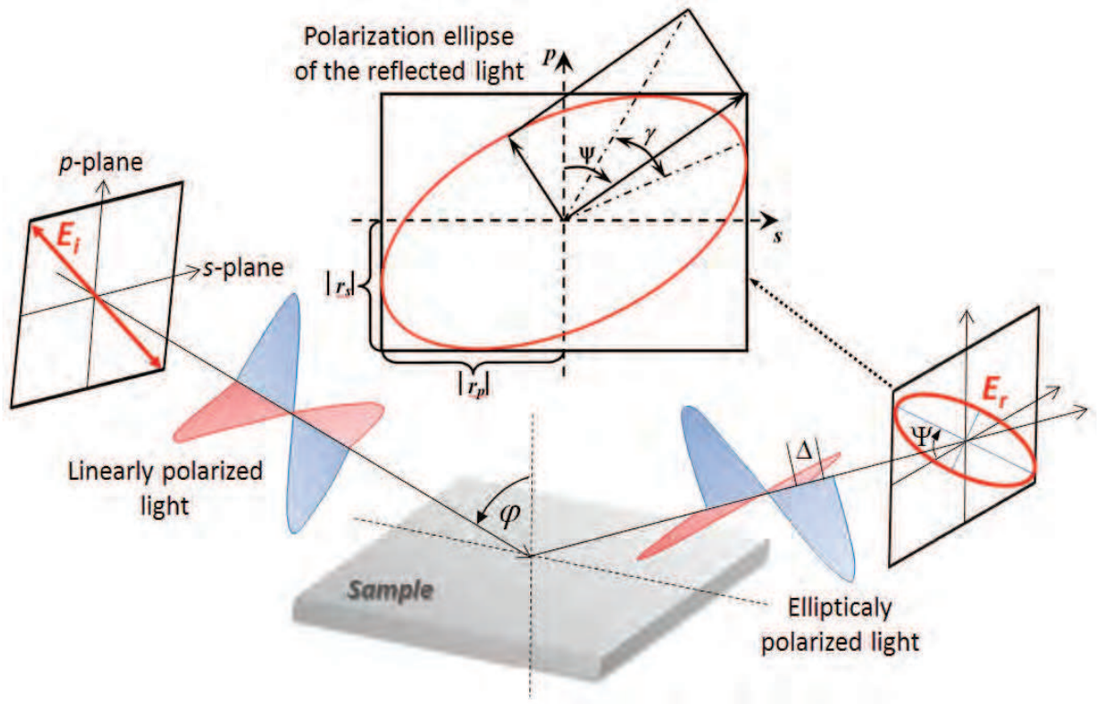

Fig. 1. Light reflecting from a sample at angle φ. The linearly polarized incident light has two electric field components E_{ip} and E_{is} in the directions parallel and perpendicular to the propagation plane, respectively. The reflected light has elliptical polarization.

The main ellipsometric angles ψ and Δ are the functions of dielectric constants of the sample: Consider the complex refractive index as $\tilde{n} = n - ik$, where n – refractive index, k – extinction coefficient, it can be written in a form of dielectric permittivity $\tilde{n} = n(1 - i\alpha) = \sqrt{\varepsilon}$ (Born, and Wolf, Cambridge University, 1999), where $\varepsilon = \varepsilon_1 - i\varepsilon_2$ - complex dielectric permittivity, and $\alpha = 4\pi k/\lambda$ - absorption coefficient. First, the dielectric permittivity is a response function, therefore $\varepsilon(-\omega) = \varepsilon^*(\omega)$. Second, from the causality principle we have the Kramers-Kronig (KK) relations (Tompkins and Irene, NY 2005)

$$\varepsilon_1(\omega) - 1 = \frac{2}{\pi} P \int_0^{+\infty} \frac{x\varepsilon_2(x)}{x^2 - \omega^2} dx \quad \text{and} \quad \varepsilon_2(\omega) = -\frac{2\omega}{\pi} P \int_0^{+\infty} \frac{\varepsilon_1(x) - 1}{x^2 - \omega^2} dx ,$$

where P – is the symbol of the main quantity of the integral. For isotropic media $\tilde{n}^2 = \varepsilon(\omega)$, $n^2 - k^2 = \varepsilon_1(\omega)$, $2nk = \varepsilon_2(\omega)$, then KK can be written in

$$n^2(\omega) - k^2(\omega) - 1 = \frac{4}{\pi} P \int_0^{+\infty} \frac{xn(x)k(x)}{x^2 - \omega^2} dx \quad \text{and} \quad n(\omega)k(\omega) = \frac{\omega}{\pi} P \int_0^{+\infty} \frac{n^2(x) - k^2(x) - 1}{x^2 - \omega^2} dx .$$

The combination of KK relations with physical arguments about the behavior of optical conducts us to the sum-rule expression.

Optical properties of materials can be modeled also by considering the field re-radiated by the induced dipoles of the classical oscillators. Such classical oscillators are Lorentz oscillator, for example. In this model the dipole radiation field interferes with the incident

field in such a way as to produce absorption or refraction. The Lorentz model assumed that an electron bound with the nucleus as a harmonic oscillator. By solving the equation of motions, distribution of the complex dielectric function can be found as $\tilde{\varepsilon}$ (Tompkins and Irene, NY 2005)

$$\tilde{\varepsilon} = \varepsilon_\infty \left(1 + \frac{A^2}{(E_c)^2 - E(E - iB)} \right).$$

The model fitting parameters ε_∞, E_c,, E, B and A are in units of energy, and they are respectively: the high-frequency lattice dielectric constant, the centre energy of the oscillator, the photon energy, the vibration frequency (broadening) of the oscillator, and the amplitude (strength) of the oscillator.

Unfortunately the Lorentz oscillator (LO) does not fit well the characteristics of the complex dielectric function at the near ultraviolet and ultraviolet (UV) regions for ferroelectrics and some semiconductors (Bungay and Tiwald, 2004; Jellison et al., 1997; Synowicki and Tiwald, 2004). LO functions were used to model molecular or lattice vibrations in the infrared (Bungay and Tiwald, 2004), complex refractive index of conductive oxides (Synowicki, 1998), metals (Brevnov and Bungay, 2005), and ferroelectrics till the absorption edge (Lappalainen et al., 2005). LO is symmetric in shape, and the high and low energy sides of the function decrease at the same rate. It is because the low energy portions of the ε' curves are most strongly affected by the area under of the curve (area is proportional to $A \cdot B$), and the peak shifts to lower energies as broadening increases. As a result LO have long asymptotic tails away from the absorption peaks and can cause unacceptable absorption artifacts in transparent regions.

Tauc-Lorentz (Jellison and Modine, 1996) and Cody-Lorentz oscillator (TLO and CLO) are more flexible functions at the fundamental band gap E_g and higher energies in the UV, since these functions rapidly decrease to zero away from their center energy and do not have long asymptotic tails as LO which can result in unwanted absorption through the band gap and below. As the result the typical absorption of dielectrics due to the electrons transition from the valence band to the conductive band at high photon energies can be very well described. Depending on the material under the studies the most suitable oscillator hast to be chosen for modeling its complex dielectric function.

2.3 Modeling of depth profile

For thin films the most interesting anomalies of the properties are related to their spatial nonuniformity. The details of this nonuniformity depend on the conditions on the film surfaces (substrates, electrodes). The most important characteristic of ferroelectric thin film is their **nonuniform polarization**. Its calculation can be performed on the base of phenomenological theory with polarization gradient in free energy density (Deineka et al., 2001; Glinchuk et al., 2000; Tilley, Gordon and Breach, Amsterdam, 1996; Wang et al., 1995;, 2002). It was found (Glinchuk et al., 2000) that dielectric susceptibility is also inhomogeneous and it can be calculated, for example, on the base of Lame equation. As a matter of the fact obtained polarization $P(z)$ profile is related to that of optical refraction index: $1/n^2 \sim (1/n_0^2)\,(1 + P(z)^2)$. Due to the proportionality of the refractive index to the square of the spontaneous polarization, the inhomogeneity of the film can be detected as a refractive index depth profile.

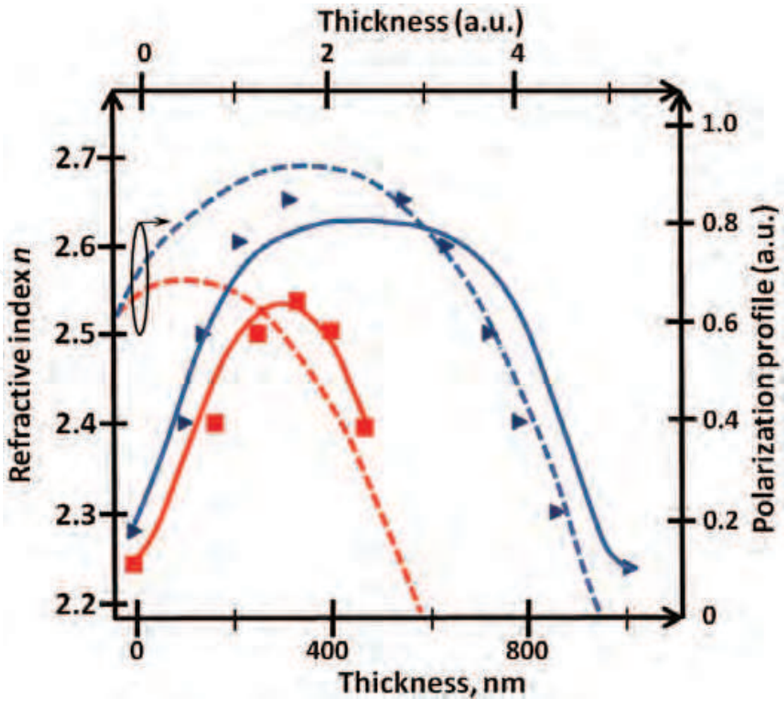

Fig. 2. Comparison the theoretically calculated (solid lines) and experimentally determined (symbols) refractive index depth profiles for PZT films of different thickness, and polarization profiles (discontinuous line) for the films with different thickness (Deineka et al., 2001).

Theoretically calculated and experimentally obtained optical profile for perovskite/pyrochlore double layer stacks of PZT (deposited using sputtering on platinized silicon wafers by Siemens AG, Munich (Germany) are presented in Fig. 2. According to theoretical prediction (Glinchuk et al., 2000), the behavior of polarization profile changes considerable for very thin PZT films. This is illustrated in Fig. 2b: the film polarization decreases monotonous with the thickness.

Polarization profile in ferroelectric thin films can be caused, e.g., during deposition, by chemical element distribution, by strains etc , and "reflected" in other physical properties of the film, for example, the refractive index profile. It should be noticed that any change in the sample structure will affect the polarization and optical properties of the material, irrespective of whether it is a result of the stoichiometry, compositional gradient, internal stresses, etc. Using spectroscopic ellipsometry it can be detected and modeled.

The depth profile of the optical properties is modeled by dividing the single layer by slices, and the shape of the grading profile is characterized using:

- Simple graded model, e.g., exponential variation of the refractive index n versus film thickness ($n \sim ab^d$);
- Function based graded model, e.g., polynomial ($n \sim A_0 + A_1 d + A_2 d^2 + \ldots$).

Some examples of the depth profile of n are represented in Fig.3.

If the film has no gradient of the refractive index, there is no change of n, and in case of the simple graded model, exponent is equal to 1. Variation of the refractive index from the substrate to the film surface is adjusted by exponent greater or smaller then 1. In this graded model the fitting parameters are value of exponent and variation of n. Optical gradient

typically is calculated in the wavelength region of 500 – 1000 nm, where ferroelectrics and dielectrics are not absorbing the light, to minimize fitting parameters correlation caused artifacts.

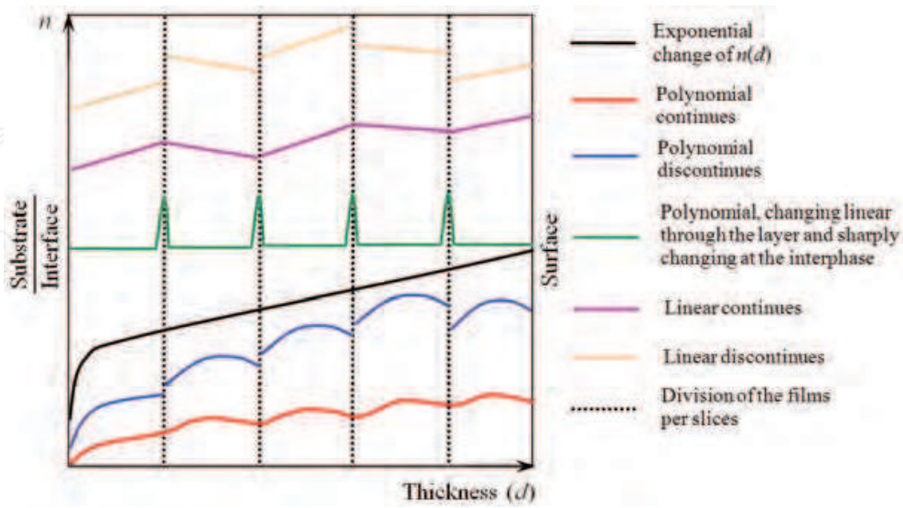

Fig. 3. The optical depth model examples applied to fit experimental SE data: exponential variation of *n* trough the film, considering it as a one complete layer; discontinues liens - exponential variation of n at the each layer of the film. The different shapes of exponent were accomplished by changing the value of exponent and variation of the refractive index.

3. Optical gradient in PZT

3.1 Optical properties of PZT films

In the Fig. 4 refractive index *n* and extinction coefficient *k* as a function of photon energy for PZT thin films with different composition are presented. These are typical dispersions of optical constant for PZT thin films with no compositional gradient. With increase of Zr/Ti ratio refractive index decreases, while optical band gap is practically not changing, suggesting that the substitution of Ti by Zr does not change much the electronic band structure of PZT.

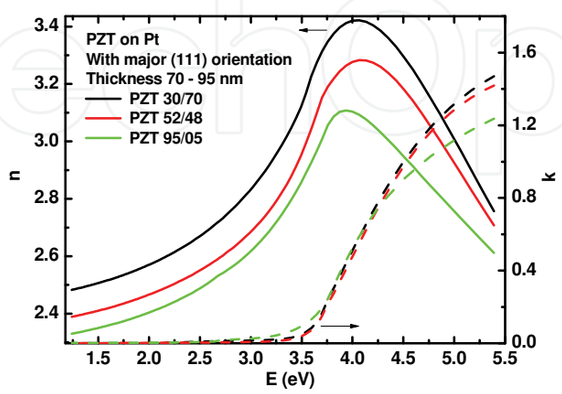

Fig. 4. Refractive index *n* and extinction coefficient *k* of sol-gel PZT thin films of 3 different compositions. Complex dielectric function of the PZT was evaluated by fitting experimental data of spectroscopic ellipsometry. *n* and *k* was modeled using Tauc-Lorentz oscillator.

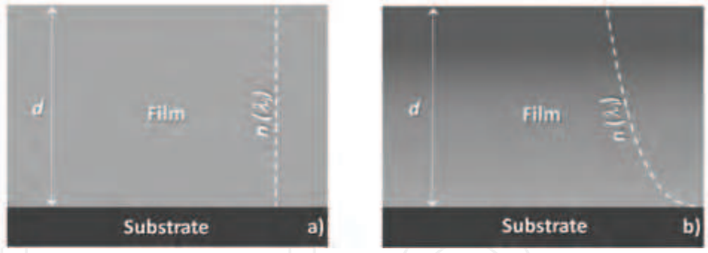

Fig. 5. Schematic illustration of the film with thickness d with a) no change of refractive index n and b) with change of n at wavelength λ_i from the bottom to the top of the film presenting optical gradient in the film. Change of n with d can have different nature (see Fig. 2), depending on the chemical/physical processes involved.

The most sensitive parameter to the composition change in PZT is refractive index, and compositional gradient can be detected as an optical gradient (e.g., refractive index change in the depth of the film). Film with no compositional gradient has no change of n and k within the film with the thickness d, while films with compositional gradient will have depth profile of optical constants as schematically presented in Fig. 5.

3.2 Factors inducing the gradient

Structural and ferroelectric properties, growth rate, phase composition, and stoichiometry of PZT films depend on a number of film deposition parameters, among which are:

- **Chemical solution deposition (CSD) or sol-gel technique:** precursor solution (lead content of the starting solution; thermal decomposition of raw components), a low-temperature heat treatment at 300-400°C (pyrolysis) to remove organic components, high-temperature annealing (600-700°C) to form a dense crystalline layer, substrate (difference in thermal expansion coefficient between the film and the bottom electrode), annealing atmosphere; how annealing was accomplished (furnace, hot plate, rapid thermal annealing etc)
- **Hydrothermal method:** Gas pressures, synthesis temperature;
- **Sputtering:** substrate temperature, gas pressure and composition, sputter power, target-to-substrate distance, and target composition;
- **Pulsed Laser Deposition (PLD):** laser parameters (laser spot size, fluence, wavelength, repetition rate, power), properties of the target material, ambient gas pressure and composition, substrate type and temperature, substrate-to-target distance and target-substrate geometry;
- **Metal-Organic Chemical Vapor Deposition (MOCVD):** substrate temperature, chamber pressure, and oxygen partial pressure.

The gradient (either compositional and/or optical) can be induced by following factors (see Fig. 6):

- Thermodynamically driven diffusion and/or kinetic demixing (Cabrera, and Mott, 1948; Impey et al., 1998; Ohba et al., 1994; Okamura et al., 1999; Wagner, 1971; Watts et al., 2001 and 2005);
- Stress (e.g., lattice mismatch and misfit stress with the substrate; stress dependence of film thickness), (Corkovic et al., 2008; Izyumskaya et al., 2007; Gkotsis et al., 2007);
- Nucleation processes (Izyumskaya et al., 2007; Ohba et al., 1994; Okamura et al., 1999).

Depending on deposition processes involved, some or even all of these factors can be incorporated and accountable for gradient formation in the films. For the same film

deposition technique different kind of chemical gradient can be obtained depending on deposition conditions.

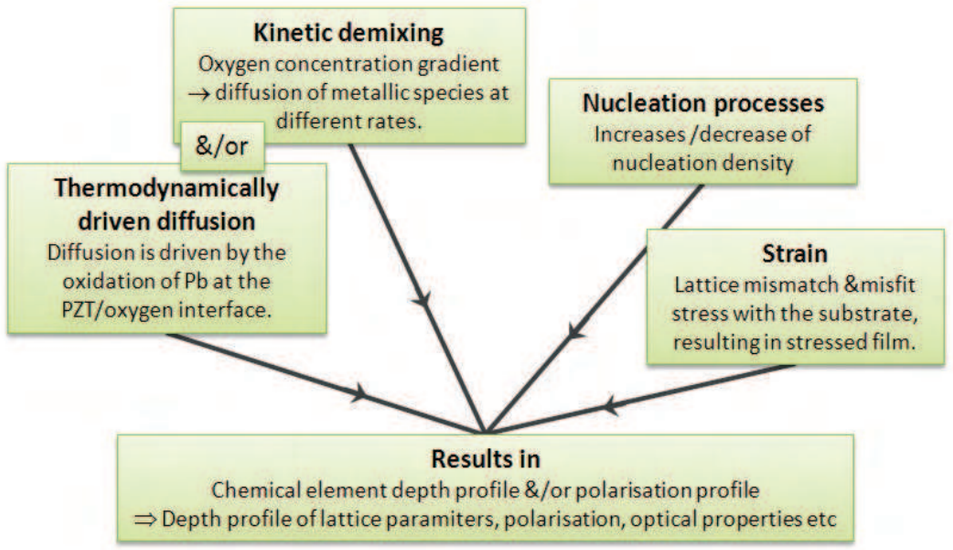

Fig. 6. Optical gradient formation reasons in thin films.

3.3 Gradient in PZT thin films prepared by sputtering and hydrothermal techniques

Some examples of compositional gradient for sputtering and hydrothermal techniques are summarized in Fig. 7. For sputtering methods it is quite common to obtain PZT films with enriched Pb and/or Pb/(Zr+Ti) towards the surface of the film resulting in increase of refractive index near the surface (Fig. 7, Case 1 and 2). It is due to the fact that sputtering techniques have difficulty in composition control due to high volatility of Pb or PbO.

Special profile of refractive index in the perovskite PZT films is induced by a selfpolarization formed during film deposition and cooling down (Deineka et al, 2001, Suchaneck et al., 2002). For example, PZT thin films of about 1 μm thickness deposited by dc and RF-sputtering on Si/SiO_2/adhesion layer/(1 1 1)Pt substrates had the Ti/Ti+Zr ratio nearly constant throughout the PZT film, while the surface was strongly lead enriched (Pb/Ti+Zr ≈ 1.6) and the bottom electrode interface was lead depleted (34). Obtained optical profile by SE was similar to that presented in Fig. 2.

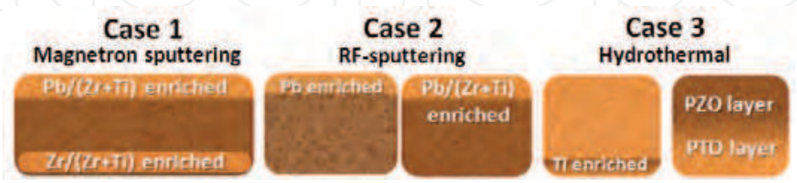

Fig. 7. Common compositional profiles for PZT thin film fabricated by sputtering and hydrothermal techniques. Case 1: based on the work of Vidyarthi et al., 2007; Case 2: Chang and He, 2005; Suchaneck et al., 2002; Case 3: Morita et al., 1997; Ohba et al., 1994.

The situation is different with hydrothermal methods where, due to the low process temperature and relatively high pressure, Pb and PbO evaporation does not take place and

interdiffusion and chemical reaction between the film and the substrate is suppressed. For example, Ohba et al., 1994, observed a steep gradient of chemical composition between a substrate and a PZT layer: an interfacial Ti-rich PZT layer with low piezoelectric constant near the substrate. Contrary to this result, Morita et al., 1997, reported that separated PTO and PZO layers were deposited during the nucleation process; the PTO layer grew during the first 2 h of the nucleation process, followed by the PZO film growth (Fig. 7, Case 3).

3.4 Gradient in sol-gel PZT thin films

A great number of sol-gel processing paramiters as temperature pyrolysis and final heat-treatment, heat treatment atmosphere and duration, solution composition, and seeding layer are strongly influencing the structural and, therefore, physical properties of PZT films. Broad studies have been done on chemical depth profile of sol-gel PZT films depending on the process conditions mention above. Some examples of chemical depth profile for sol-gel PZT films on platinized Si (regarding solvents, pyrolysis and annealing) are given in Fig.8. As can be seen it is not evident whether initial sol or annealing is responsible for the gradient appearance. One of the major limitations of the sol-gel technique is that it does not yield the desired perovskite phase directly. Thermodynamically driven diffusion and/or kinetic demixing for sol-gel films are strongly determine by how the annealing is accomplished (furnace, hot plate, rapid thermal annealing, temperature, duration etc), lead content of the starting solution, and also thermal decomposition of raw components. Quite often some of these factors are not mentioned in the publications and it makes difficult or even impossible to do comparisons and reasonable conclusions of these studies.

The formation of perovskite phase upon final annealing is preceded by an undesirable nonferroelectric pyrochlore phase. Pyrochlore inclusions are often observed in sol-gel derived perovskite films. An intermediate annealing step (pyrolysis) plays a pivotal role in determining the crystal orientation as well as ferroelectric and piezoelectric properties of the resultant PZT films (Izyumskaya et al., 2007). There are some studies done for this intermediate stage.

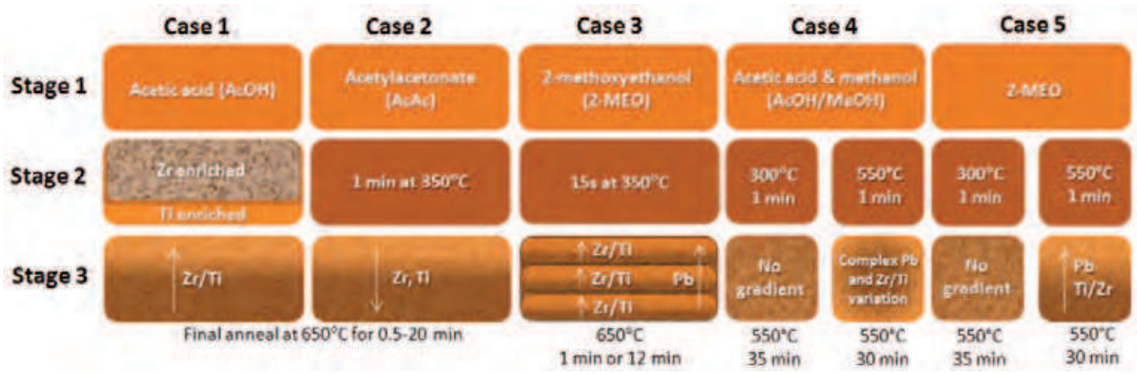

Fig. 8. Common compositional profiles for PZT thin film fabricated by sol-gel. Stage 1: Initial gel; Stage 2: Initial crystallization; Stage 3: Full crystallization. Case 1 and 2: based on work of Etin et al., 2006; Case 3: Ledermann et al., 2004; Case 4 and 5: Aulika et al., 2009.

The paper of Etin et al., 2006, proved that variation in Zr/Ti ratio in PZT films originates early in the crystallization process. These variations are caused by a mismatch in the thermal decomposition of the individual Zr/Ti components in the PZT precursor. Once created, the

compositional gradients cannot be eradicated by prolonged heat treatments. In the Cases 1 and 2, presented in Fig, 8, PZT films were prepared by two sol-gel precursor formulations. The difference between the two formulations is the stabilization of the zirconium precursor: a) Zr precursor is chemically stabilized with AcOH, or b) Zr is stabilized with acetylacetonate (AcAc). Formulation (a) led to opposite concentration gradients of Zr (increasing) and Ti (decreasing) towards surface, while formulation (b) gave rise to constant Zr and Ti concentrations towards the substrate throughout the films. The elemental depth distributions are governed by the thermal decomposition pattern of the individual metal compounds in the sol–gel precursor (Etin et al., 2006). In formulation (a) Zr precursor stabilized with AcOH showed faster pyrolysis and lower decomposition temperature than the Ti precursor. Thus, in formulation (a) Zr-rich phase can form in the bulk before the Ti precursor enters the reaction. After the Ti precursor decomposes, growth of Ti-rich PZT film proceeds from the interface with the Pt electrode leading to opposing concentrations gradients of Zr and Ti in the film. In formulation (b) the decomposition of Ti and Zr precursors occurs simultaneously and therefore a uniform depth profile is obtained.

Distribution of the nearest neighbor and next nearest neighbor ions in the pyrochlore phase was demonstrated to be similar to those in the amorphous phase (Reaney et al., 1998). Therefore, although perovskite is the thermodynamically stable phase in the temperature range used in sol-gel fabrication, the transformation from amorphous to pyrochlore phase is kinetically more favorable than a straight transformation to the perovskite phase. The kinetics of transformation from the amorphous to perovskite phase as well as film orientation was shown to depend strongly on the pyrolysis conditions (Brooks et al., 1994; Reaney et al., 1998).

In the work of Ledermann et al., 2003, it is shown that sol-gel PZT thin films are Ti-rich closer to the substrate and Zr-rich closer to the surface for each layer of the film, as well as that the concentration of Pb increases directionally from the substrate to the surface (Fig. 8, Case 3). This is special case of controlled compositional gradient of sol-gel PZT thin films: the gradient has amplitude of ±20% at the 53/47 morphotropic phase boundary (MPB), showing improved electrical performances. Thanks to the high development of film deposition techniques, in our days it is possible to fabricate controlled compositions, textures and structures of the films with dedicated properties.

These gradient studies show that selection of precursors (chemical solvents) and processing parameters (drying temperatures and time, crystallization temperature and time, etc.) for the deposition of sol-gel films is influential in controlling the homogeneity of the films.

Recently detailed studies of sol-gel PZT 52/48 thin and thick films were presented (Aulika et al., 2009), which were made by using two different solvent systems: a mixture of acetic acid and methanol (AcOH/MeOH) or 2-Methoxyethanol (2-MEO) (Fig. 8, Case 4 and 5). To crystallize the films, two different thermal profiles were applied: all layers crystallized together (LCT) at the same time, and each layer crystallized individually (LCI). The first profile employed the deposition of one layer followed by drying at 300°C for 1 min. When the final layer was deposited, the sample was placed on a hotplate at 550°C for 35 min to crystallize. The second thermal profile involved individual crystallization of each layer by holding the sample at 300°C for 1 min followed by 550°C for 5 min before the next layer was coated. The annealing time was sufficient for all films to crystallize.

Among all analyzed samples, the refractive index gradient was found only for two groups of films, which were made by crystallizing each layer before another layer was deposited (LCI) (Aulika et al., 2009): 1) One group of films was made using the AcOH/MeOH sol

(Fig. 9a) and 2) the other group was made with the 2-MEO sol (Fig. 9b). The gradient is different for all films of different thickness (Fig. 9). This is most likely due to recurrent annealing of already crystallized layers. The trend of *n* with depth presented in Fig. 9b can be caused by several reasons such as 1) residual stress in the film, 2) concentration gradients of Ti or Zr with the layer, 3) an increase in excess Pb (Aulika et al., 2009; Deineka et al., 2001; Ledermann et al., 2003; Watts et al., 2005), 4) polarization profile that is strongly dependent on film thickness (polarization is homogeneous in the greater part of the thick film except in small regions at the film boundaries, while it is completely inhomogeneous in thin films).

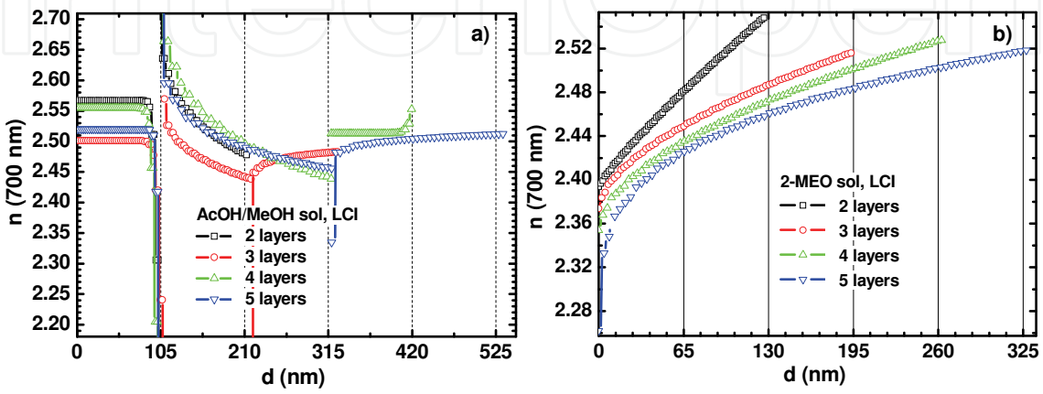

Fig. 9. Depth profile of refractive index n at the 700 nm of wavelength for the samples with different number of layers made using a) AcOH/MeOH, and b) 2-MEO sol. All figures taken from (Aulika et al., 2009). © The Electrochemical Society, Inc. [2009]. All rights reserved.

No optical gradient is found for films with different numbers of layers when all layers are crystallized at the same time, regardless of the sol used. This was also confirmed for the tick films (Aulika et al., 2009). The groups of films made with AcOH/MeOH sol and by the LCT routine show strong (111) orientation with some low intensity peaks of other orientations, such as (110), (112) or (001)/(100) (Fig. 10 cd). While films with optical gradient revealed (001)/(100) and (002)/(200) orientations (Fig. 10 ab).

Based on the XRD results (Aulika et al., 2009) of LCI films, a picture of how the orientation of the film changes when more layers are added was obtained. Thus, when processing the films using the LCI method, only the first layer crystallizes directly on the Pt substrate and all subsequently deposited layers crystallize on top of PZT 52/48. Since the thermal profile used assures (100) orientation of the film, we would expect the first layer to be (100) oriented, as well as all subsequently deposited layers, since the last layer also is crystallize on (100) PZT. Nevertheless, both groups of PZT 52/48 films processed with the LCI method in fact exhibit some (111) orientation for films having more than three layers. The appearance of (111) orientation can only be explained if some excess of PbO after crystallization is assumed, located close to the surface, as recently reported by Brennecka et al., 2008. Indeed, some pyrochlore was found for all LCI films made with AcOH/MeOH sol. It is thus possible that after the deposition of the next layer, the residual pyrochlore induced nucleation and growth in the (111) direction, consuming the uncrystallized matrix and accounting for the appearance of the (111) orientation at later stages within the first layer. Considering the work of Brennecka et al., 2008 and results of Aulika et al., 2009, the uncrystallized pyrochlore phase was most likely the lead deficient fluorite phase, which was also accompanied by a compositional gradient of Pb/Zr through the layer thickness.

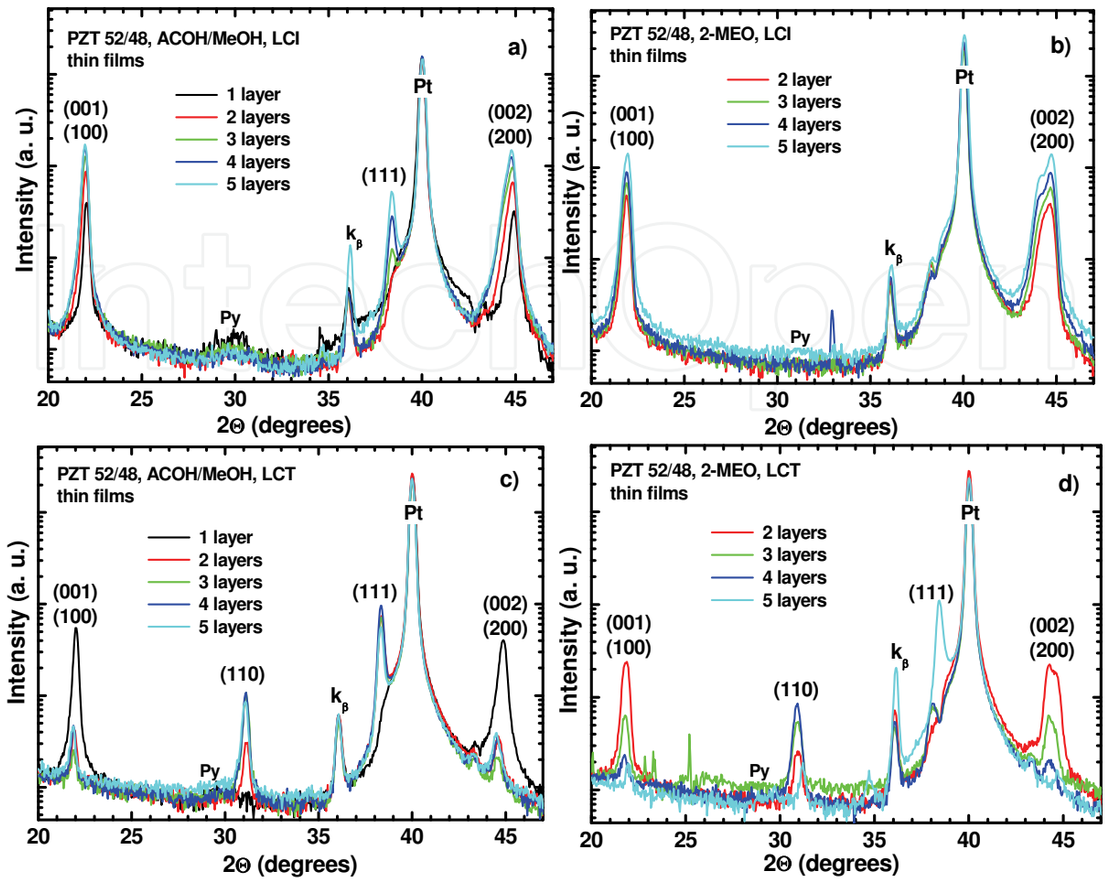

Fig. 10. The XRD of the LCI samples for a) AcOH/MeOH films, b) 2-MEO films, and LCT samples for c) ACOH/MeOH films, and d) 2-MEO films. All figures taken from (Aulika et al., 2009). © The Electrochemical Society, Inc. [2009]. All rights reserved.

In pinpointing the cause of the detected optical gradient, any change in orientation with number of layers can be eliminated based on the consideration that the films made with the LCT method showed more mixed orientation among the samples, and yet no optical gradient was found for these films. Moreover, the optical gradient was found in films made with the LCI route, where a strong variation in lattice parameter with increasing thickness was found, even though the type of gradient was dependent on the sol used.

On the other hand, it was reported that the *n* increases with increasing Ti/Zr concentration (Tang et al., 2007; Yang et al., 2006). It is likely that the appearance of the depth profile for the LCI films is connected with the fact that $PbTiO_3$ (PTO) crystallizes before $PbZrO_3$ (PZO) (Impey et al., 1998), while crystallizing layers together may avoid preferential PTO and PZO crystallization. Better quality PZT 52/48 composition thin films can be made by annealing the films at higher temperatures using rapid thermal annealing (RTA) or oven, or to have a different Zr/Ti concentration ratio in each layer with the goal to anticipate the selection and diffusion processes (Calamea and Muralt, 2007). RTA usually needs fully crystallizing at > 650°C, but in the study of Aulika et al., 2009, annealing temperature at 550°C on a hotplate was chosen so that the crystallization of the films started at the interface of Pt/ PZT and grew up to the top rather than crystallizing the films in a oven/RTA which would lead to the crystallization from everywhere and smeared the possible formation of gradient in

composition. This use of low annealing temperature led to the formation of pyrochlore (Fig. 10a, c).
To summarize, there are three possible origins of the refractive index gradient $n(d)$: 1) the above-mentioned polarization inhomogeneity close to the film surface, and 2) the varying Zr/Ti ratio and 3) varying Pb throughout the layer. The latter two can be attributed to the separate crystallization of each layer, causing the diffusion of Pb, Ti and Zr ions in the film.
If we extrapolate this to the optical properties according to the fact that n increases with decreasing Zr/Ti ratio (Fig.3), then we can say from Fig. 8b that the Zr/Ti ratio decreases directionally from the substrate to the surface, which is opposite to the observations, e.g., of Ledermann by TEM. However, it is known that sol-gel thin films may have higher concentrations of Pb at the surface (Impey et al., 1998; Ledermann et al., 2003; Watts et al., 2005).

3.4.1 Surface enrichment in ferroelectric thin films

Surface enrichment of some elements has been reported by many authors (Impey et al., 1998, Watts et al., 2001, 2003 and 2005; Gusmano et al., 2002), and there are just few explanations for this phenomenon. An analogy may be drawn with the oxidation of metals such as Cu and Sn where the metals dif-fuse towards the reacting surface (Wagner, 1971; Cabrera and Mott, 1948).
The data presented by Watts et al indicates that the pyrolysis and crystallization steps for sol-gel films result in incomplete oxidation (Watts et al., 2005). The diffusion is driven by the oxidation of Pb at the PZT/oxygen interface. The second mechanism is kinetic demixing (Martin, 2003): diffusion of metallic species at different rates, usually in the direction of higher oxygen potential (even though the phase is thermodynamically stable under all these oxygen pressures). This mechanism is often applied for kinetics of solid solutions, but it was shown that a single phase can decompose under a chemical potential gradient (Wang and Akbar, 1992). Most likely that both processed (thermodynamically driven diffusion or kinetic demixing, (Fig. 6) are taking place since it is difficult to separate them due to the fact that the low oxygen content in the film promotes both processes.

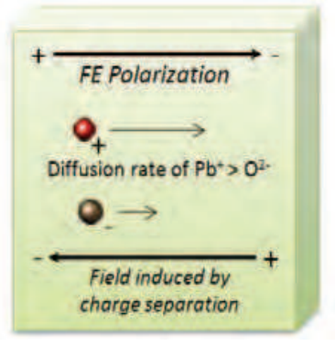

Fig. 11. Self-poling mechanism in ferroelectric thin films.

An electrical potential that polarizes the ferroelectric at high temperatures as it cools through the Curie temperature is created by the migration of cations in the film (Fig. 11). The spontaneous polarization allows the cations to diffuse faster and is the reason why surface enrichment is so significant in ferroelectric films (Watts et al., 2005). The ferroelectric (FE) polarization induced electrochemically by this mechanism is in the direction observed experimentally by Impey et al., 1998, and by Okamura et al., 1999. Pb^{2+} diffusion may also lead to self-polarization, which causes the polarization inhomogeneity discussed above.

3.4.2 Confirmation of optically detected gradient by TEM and EDX

Fine grains of pyrochlore phase between perovskite crystallites throughout the film thickness were observed for films made by LCI (Fig. 12a). A pyrochlore layer about 50 nm thick was found at the surface of the film. These results are in accordance with the XRD analysis (Fig. 10). The EDX results showed a strong variation in Pb and Zr concentrations throughout the thickness of the film (Fig. 12b), and this film had a strong optical gradient. Close to the surface where the pyrochlore layer was observed, a strong reduction in lead concentration and an increase in zirconium concentration were detected.The titanium concentration was not much affected by the phase separation. It can be conclude that these samples show the same two-phase structure reported by Brennecka et al within each layer, whereby the lead-deficient upper layer causes a compositional gradient.

For PZT 52/48 (LCT) film the columnar grains and additional ~10 nm thin pyrochlore layer on the surface was found (Fig. 12c). This film had no optical gradient. No Py was detected by XRD analysis due to its low amount (see Fig. 10). As shown in Fig. 12d, a more uniform EDX concentration profile was obtained in comparison to Fig. 12b.

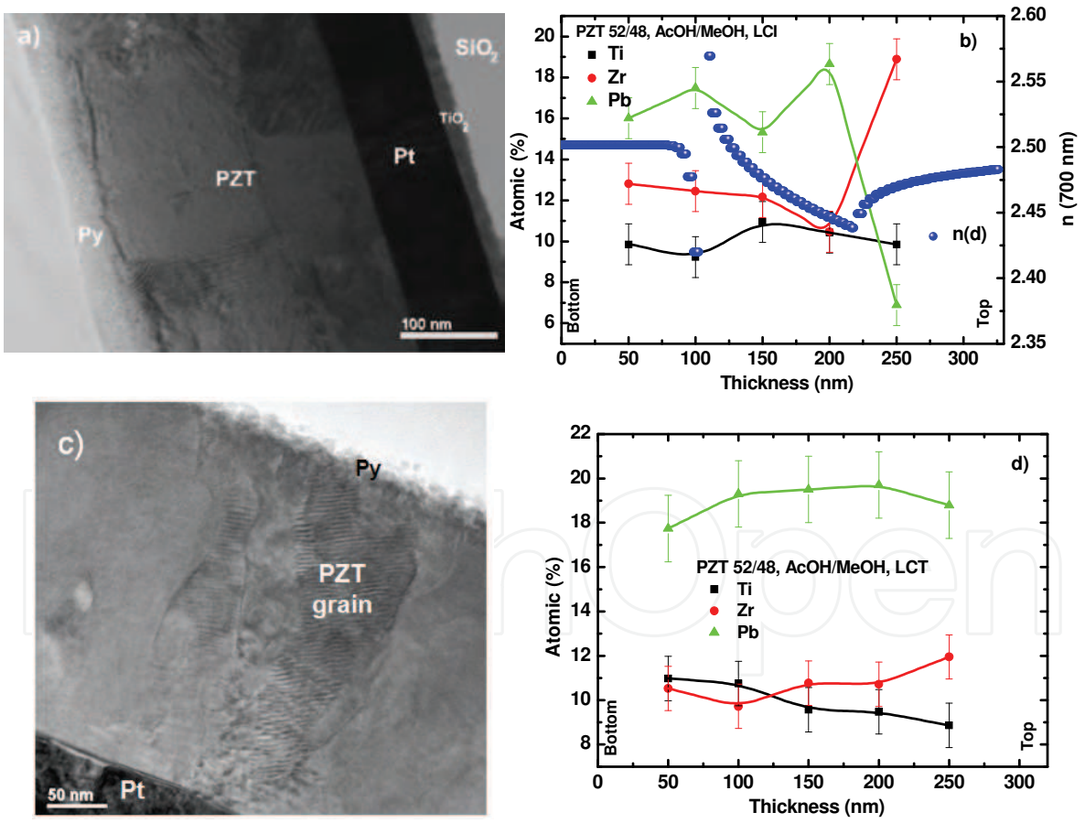

Fig. 12. TEM micrograph (dark field (a) and bright field (c)) of a cross-section of LCI film (a) and LCT film (c) showing pyrochlore phase (Py) between and on the surface of the PZT grains; EDX profile from substrate to the film surface (b, d) in comparison with the optical depth profile $n(d)$ established by SE (b). All figures taken from (Aulika et al., 2009). © The Electrochemical Society, Inc. [2009]. All rights reserved.

The results obtained by EDX are in good agreement with the optical data evaluated by SE (Fig. 12b). There are almost no changes in variation of Pb, Zr, and Ti near the substrate of the film, which is "reflected" in optical analyses as no optical gradient $n(d)$. A significant decrease in Pb and increase in Zr can be seen in the optical data as a decrease in $n(d)$. Near the surface $n(d)$ starts to increase, which is in good agreement with other results (Deineka et al., 1999, 2001, and January 2001; Suchaneck et al., 2002).

4. Conclusion

The brief introduction into the composition problems and composition control of $Pb(Zr_xTi_{1-x})O_3$ (PZT) films were laid out in this chapter. Structural and ferroelectric properties, growth rate, phase composition, and stoichiometry of PZT films depend on a number of film deposition parameters. Understanding the chemistry and physics behind the formation of PZT films are of basic and technological importance. The gradient (either compositional and/or optical) can be induced by such factors as thermodynamically driven diffusion and/or kinetic demixing, stress, and nucleation processes. Depending on deposition processes involved, some or even all of these factors can be incorporated and accountable for compositional and/or optical gradient formation in the films. For the same film deposition technique different kind of chemical gradient can be obtained depending on deposition parameters. Any change in the sample structure will affect the polarization and optical properties of the material, irrespective of whether it is a result of the stoichiometry, compositional gradient, internal stresses, etc.

Examples on the characterization methods both intrusive and nondestructive were given, underlining the advantages of optical methods, especially spectroscopic ellipsometry, for gradient detection in films.

The depth profile of the refractive index and composition was presented in details for sol-gel PZT 52/48 thin films made using different chemical solvents and annealing procedures. Thanks to the high development of film deposition techniques, in our days it is possible to fabricate controlled compositions, textures and structures of the films with dedicated and improved electrical properties.

It was also demonstrated that separate crystallization of the layers determines the gradient appearance, irrespective of the chemical solvents as AcOH/MeOH and 2-MEO. The analysis of the XRD results of PZT 52/48 films made with LCI has shown that these films have a preferred orientation of (001)/(100) in contrast to the films made with LCT, which have shown a predominant (111) orientation and no gradient in optical properties. A more refined analysis has shown that a refractive index gradient was apparent in the samples in which lattice parameters strongly change with thickness. For these films, EDX analysis showed significant variation in Pb and Zr. In addition, these qualitative spectroscopic ellipsometry analyses are in accordance with results obtained with other methods, like EDX and ERD. Thus, the spectroscopic ellipsometry method offers the opportunity to accomplish quality analysis of thin films in a relatively simple, fast, and non-destructive way.

To improve spectroscopic ellipsometry calculation for PZT films with complex optical gradients, the films should be considered as a media of two materials – PZT 52/48 and Py, where the $PbTiO_3$ and $PbZrO_3$ concentrations change within a PZT film. Such complex calculations can be obtained from SE experimental data if additional SE measurements are made on samples of pure Py, $PbTiO_3$ and $PbZrO_3$ films to extract their optical properties. Nevertheless, by applying a simple exponential gradient model to experimental SE data

analysis, reasonable qualitative data can be obtained which gives an idea of the quality of the sample, its optical properties, optical gradient and homogeneity. Moreover, these qualitative SE analyses are in accordance with results obtained with other methods, e.g., SIMS, EDX and XRD. Thus, the SE method offers the opportunity to accomplish optical analyses of thin films in a simple, fast, precise and non-destructive way, as well as acquire reasonable results and obtain justified information about the quality of thin films. SE is perfect also for real time monitoring of film growth, thickness, optical constants, interface, roughness, optical gradient detection.

Advantages of SE like speed and accuracy, nondestructiveness, no specific sample preparation requirements, compatible with liquid & solid samples, characterization on both absorbing & transparent substrates, thermo-optics (e.g., phase transition analyses), and inhomogeneities detection (porosity, surface roughness, interfaces, optical gradient etc) is of great significance not only from a fundamental, but also from a technological point of view due to intense developments in micro & nano-electronics for nanostructures engineering, where changes in interfaces, within the films and surfaces, and a requirement to detect it, plays very important role. And in this spectroscopic ellipsometry is unique as metrology instrumentation.

5. Acknowledgements

Some results published in this chapter were made within the 6th Framework Program of the Multifunctional & Integrated Piezoelectric Devices (MIND). This work was supported by the European Social Fund and UNESCO LÓREAL Latvian National Fellowship for Woman in Science, and grants KAN301370701 of the ASCR, 1M06002 of the MSMT CR, 2 202/09/J017 of GACR and AV0Z10100522. We would like to express our gratitude to Sebastjan Glinsek for TEM sample preparation.

6. References

Aulika, I.; Corkovic, S.; Bencan, A.; D'Astorg, S.; Dejneka, A.; Zhang, Q.; Kosec M.; Zauls, V. (2009), The influence of processing parameters on the formation of optical gradients in chemical solution-derived $PbZr_{0.52}Ti_{0.48}O_3$ thin films. *Journal of Electrochemical Society*, 156, G217

Aulika, I.; Dejneka, A.; Lynnyk, A.; Zauls, V.; Kundzins, M. (2009), Thermo-optical investigations of $NaNbO_3$ thin films by spectral ellipsometry. *Physica Status Solidi (c)*, 6, 2765

Aulika, I.; Dejneka, A.; Zauls, V.; Kundzins, K. (2008), Optical gradient of the trapezium-shaped $NaNbO_3$ thin films studied by spectroscopic ellipsometry, *Journal of Electrochemical Society*, 155, G209

Aulika, I.; Deyneka, A.; Zauls V.; Kundzins, K. (2007), Thermo-optical studies of $NaNbO_3$ thin films. *Journal of Physics, Conference Edition,* V93, 012016

Boher, P.; Stehle, J. L.; Piel, J. P.; Fried, M.; Lohner, T.; Polgar, O.; Khanh, N. Q.; Barsony, I. (1996), Spectroscopic ellipsometry applied to the determination of an ion implantation depth profile. *Nuclear Instruments and Methods in Physics Research Section B,* 112, 160

Born, M.; Wolf, E. (Cambrig University, 1999), *Principles of optics*, 7th *(expended) edition*

Bovard, B.G. (1990), Rugate filter design: the modified Fourier transform technique, *Applied Opt*ics, 29, 24-30

Brennecka, G.L.; Parish, C. M.; Tuttle, B. A.; Brewer, L. N.; Rodriguez, M.A. (2008), Reversibility of the Perovskite-to-Fluorite Phase Transformation in Lead-Based Thin and Ultrathin Films. *Advanced Mate*rials, 20, 1407

Brevnov, D. A.; Bungay, C. (2005), Diameter-Dependent Optical Constants of Gold Mesoparticles Electrodeposited on Aluminum Films Containing Copper. *The Journal of Physical Chemistry B,* 109, 14529

Brooks, K. G.; Reaney, I. M.; Klissurska, R.; Huang, Y.; Buzsill, L.; Setter, N. (1994), Orientation of rapid thermally annealed lead zirconate titanate thin films on (111) Pt substrates. *Journal of Material Research,* 9, 2540

Bungay, C.; Tiwald, T. E.; (2004), Infrared spectroscopic ellipsometry study of molecular orientation induced anisotropy in polymer substrates. *Thin Solid Film,* 455 – 456 272;

Cabrera, N.; Mott, N. F (1948), Theory of the Oxidation of Metals. *Reports on Progress in Physics,* 12, 163–184

Calamea, F.; Muralt, P. (2007), Growth and properties of gradient free sol-gel lead zirconate titanate thin films. *Applied Physics Lett*ers, 90, 062907

Callard, S.; Gagnaire, A.; Joseph, J. (1998), Characterization of graded refractive index silicon oxynitride thin films by spectroscopic ellipsometry. *Thin Solid Films,* 313-314, 384

Chang, W.L.; He, J.L. (2005), Comparison of the microstructures and ferroelectric characteristics of sputter deposited PZT films with and without lead or lead oxide for compensation. *Ceramics International,* 31, 461–468

Corkovic, S.; Whatmore, R. W.; Zhang, Q. (2008), Development of residual stress in sol-gel derived $Pb(Zr,Ti)O_3$ films: An experimental study. *Journal Applied Physics,* 103, 084101

Deineka, A. M.; Glinchuk, D.; Jastrabik, L.; Suchaneck, G.; Gerlach, G. (January, 2001), Nondestructive investigations of the depth profile of PZT ferroelectric films. *Ferroelectrics* 264, 151

Deineka, A.; Glinchuk, M. D.; Jastrabik, L.; Suchaneck, G.; Gerlach, G. (2001), Ellipsometry investigation of perovskite/pyrochlore PZT thin film stacks. *Ferroelectrics* 258, 271

Deineka, A.; Glinchuk, M.; Jastrabik, L.; Suchaneck, G.; Gerlach, G. (2001), Ellipsometric Investigations of the Refractive Index Depth Profile in PZT Thin Films. *Physica Status Solidi A,* 188, 1549

Deineka, A.; Jastrabik, L.; Suchaneck, G.; Gerlach, G. (1999), Optical Properties of Self-Polarized PZT Ferroelectric Films. *Ferroelectrics,* 273, 155-160

Dejneka, A.; Aulika, I.; Makarova, M. V.; Hubicka, Z.; Churpita, A.; Chvostova, D.; Jastrabik, L.; Trepakov, V. A. (2010), Optical Spectra and Direct Optical Transitions in Amorphous and Crystalline ZnO Thin Films and Powders. *Journal of Electrochemical Society,* 157, G67

Dejneka, A.; Aulika, I.; Trepakov, V.; Krepelka, J.; Jastrabik, L.; Hubicka, Z.; Lynnyk, A.; (2009), Spectroscopic ellipsometry applied to phase transitions in solids: possibilities and limitations. *Optics Express*, 3 14322

Etin, A.; Shter, G. E.; Baltianski, S.; Grader, G. S.; Reisner, G. M. (2006), Controlled Elemental Depth Profile in Sol–Gel-Derived PZT Films, *Journal of American Ceramic Society*, 89, 2387–2393

Fried, M.; Petrik, P.; Lohner, T.; Khánh, N. Q.; Polgár O.; Gyulai, J. (2004), Dose-dependence of ion implantation-caused damage in silicon measured by ellipsometry and backscattering spectrometry. *Thin Solid Films* 455-456, 404

Gibbons, B.J.; Trolier-McKinstry, S. (1999), The sensitivity limits of spectroscopic ellipsometry to oxygen content in YBa2Cu3O7-d thin films. *Thin Solid Films* 352, 205

Gkotsis, P.; Kirby, P.B.; Saharil, F.; Oberhammer, J.; Stemme, G. (2007), Thin film crystal growth template removal: Application to stress reduction in lead zirconate titanate microstructures. *Applied Physics Lett*ers, 91, 163504

Glinchuk, M. D.; Eliseev, E. A.; Deineka, A.; Jastrabik, L. (2000), Optical refraction index and electric polarization profile of ferroelectric thin film. *Fine mechanics and optics*, 45, 338-342

Glinchuk, M. D.; Eliseeva, E.A.; Stephanovich, V.A. (2002), The depolarization field effect on the thin ferroelectric films properties. *Physica B*, 322, 356–370

Guenther, M.; Gerlach, G.; Suchaneck, G.; Sahre, K.; Eichhorn, K.-J.; Wolf, B.; Deineka, A.; Jastrabik, L. (2002), Ion-beam induced chemical and structural modification in polymers. *Surface and Coatings Technology,* 158-159, 108

Gusmano, G.; Bianco, A.; Viticoli, M.; Kaciulis, S.; Mattogno, G.; Pandolfi, L., (2002), Study of $Zr_{1-x}Sn_xTiO_4$ thin films prepared by a polymeric precursor route. *Surface and Interface Analysis*, 34, 690–693

Impey, S. A.; Huang, Z.; Patel, A.; Beanland, R.; Shorrocks, N. M.; Watton, R.; Whatmore, R. W. (1998), Microstructural characterization of sol-gel lead-zirconate-titanate thin films. *Journal of Applied Physics,* 83, 2202

Izyumskaya, N.; Alivov, Y.-I.; Cho, S.-J.; Morkoc, H.; Lee, H.; Kang, Y.-S. (2007), Processing, Structure, Properties, and Applications of PZT Thin Films. *Critical Reviews in Solid State and Materials Sciences*, 32, 111-202

Jellison, G. E.; Modine, F. A. (1996), Parameterization of the optical functions of amorphous materials in the interband region. *Applied Physics Lett*ers, 69, 371

Jellison, G. E.; Modine, F. A.; Boatner, L. A. (1997), Measurement of the optical functions of uniaxial materials by two-modulator generalized ellipsometry: rutile (TiO_2), *Optics Letters,* 22**,** 1808

Kamp, D. A.; DeVilbiss, A. D.; Philpy, S. C.; Derbenwick, G. F. (2004), Adaptable ferroelectric memories for space applications. IEEE, Non-Volatile Memory Technology Symposium 2004, 10.1109/NVMT.2004.1380832

Lappalainen, J.; Hiltunen, J.; Lantto, V. (2005), Characterization of optical properties of nanocrystalline doped PZT thin films. *Journal of European Ceramic Society,* 25, 2273

Ledermann, N. ; Muralt, P. ; Baborowski, J.; Gentil, S.; Mukati, K.; Cantoni, M.; Seifert, A.; Setter, N. (2003), {1 0 0}-Textured, piezoelectric $Pb(Zr_x, Ti_{1-x})O_3$ thin films for MEMS: integration, deposition and properties. *Sensors and Actuators A,* 105, 162–170

Losurdo, M. (2004), Relationships among surface processing at the nanometer scale, nanostructure and optical properties of thin oxide films. *Thin Solid Films,* 455-456, 301

Marcus, R. K.; Schwartz, R. W. (2000), Compositional profiling of solution-deposited lead zirconate–titanate thin films by radio-frequency glow discharge atomic emission spectroscopy (rf-GD-AES), *Chemical Physics Letters,* 318, 481–487

Martin, M. (2003), Materials in thermodynamic potential gradients. *Journal of Chemical Thermodynamics*, 8, 1291–1308.

Morita, T.; Kanda, T.; Yamagata, Y.; Kurosawa, M.; Higuchi, T. (1997), Single process to deposit lead zirconate titanate (PZT) thin film by a hydrothermal method. *Japanese Journal of Applied Physics*, 36, 2998

Morozovskaa, A. N.; Eliseevb, E. A.; Glinchuk, M. D. (2007), Size effects and depolarization field influence on the phase diagrams of cylindrical ferroelectric nanoparticles. *Physica B*, 387, 358–366

Morton, D. E.; Johs B.; Hale, J. (2002), Soc. of Vac. Coat. 505/856-7188, *45th Ann. Techn. Conf. Proc*. ISSN 0737-5921, 1

Muralt, P. (2000), Ferroelectric thin films for micro-sensors and actuators: A review. IOPscience::.. *Journal of Micromechanics and Microengineering*, 10, 136-146

Nguyen Van, V.; Brunet-Bruneau, A.; Fisson, S.; Frigerio, J. M.; Vuye, G.; Wang, Y.; Abelvs, F.; Rivory, J.; Berger, M.; Chaton, P. (1996), Determination of refractive-index profiles by a combination of visible and infrared ellipsometry measurements. *Applied Opt*ics, 35, 5540

Nishizawa, H.; Tateyama, Y.; Saitoh, T. (2004), Ellipsometry characterization of oxidized copper layers for chemical mechanical polishing process. *Thin Solid Films,* 455-456, 491

Ohba, Y.; Arita, K.; Tsurumi, T.; Daimon, M. (1994), Analysis of interfacial phase between substrates and lead zirconate titanate thin films synthesized by hydrothermal method. *Japanese Journal of Applied Physics*, 33, 5305

Okamura, S.; Miyata, S.; Mizutani, Y.; Nishida, T.; Shiosaki, T. (1999), Conspicuous voltage shift of D–E hysteresis loop and asymmetric depolarization in Pb-based ferroelectric thin films. *Japanese Journal of Applied Physics*, 38, 5364–5367

Okamura, S.; Miyata, S.; Mizutani, Y.; Nishida, T; Shiosaki, T. (1999), Conspicuous voltage shift of D–E hysteresis loop and asymmetric depolarization in Pb-based ferroelectric thin films. *Japanese Journal of Applied Physics*, 38, 5364–5367

Oulette, M. F.; Lang, R. V; Yan, K. L.; Bertram, R. W.; Owle, R. S.; Vincent, D. (1991), Experimental studies of inhomogeneous coatings for optical applications. *Journal of Vacuum Science and Technology A,* 9, 1188- 1192

Parish, C. M.; Brennecka, G. L.; Tuttle, B. A.; Brewer, L. N. (2008), Quantitative X-Ray Spectrum Imaging of Lead Lanthanum Zirconate Titanate PLZT Thin-Films. *Journal of American Ceramic Society*, 91, 3690

Philpy, S. C.; Kamp D. A.; Derbenwick G. F. (2003), Hardened By Design Ferroelectric Memories for Space Applications," Non-Volatile Memory Technology Symposium 2003, San Diego, California

Reaney, I. M.; Taylor, D. V.; Brooks, K. G. (1998), Ferroelectric PZT thin films by sol-gel deposition. *Journal of Sol-Gel Science and Technol*ogy, 13, 813

Rivory, J. (1998), Characterization of inhomogeneous dielectric films by spectroscopic ellipsometry. *Thin Solid Films,* 313-314, 333

Snyder, P.G.; Xiong, Y.-M.; Woollam, J.A.; Al-Jumaily G.A.; Gagliardi, F.J. (1992), Graded refractive index silicon oxynitride thin film characterized by spectroscopic ellipsometry. *Journal of Vacuum Science and Technology A,* 10, 1462

Sternberg, A.; Krumins, A.; Kundzins, K.; Zauls, V.; Aulika, I.; Cakare, L.; Bittner, R.; Weber, H.; Humer, K.; Lesnyh, D.; Kulikov D.; Trushin, Y. (2003), Irradiation effects in lead zirconate thin films. Proceedings of SPIE, 5122, 341

Suchaneck, G.; Lin, W. -M.; Koehler, R.; Sandner, T.; Gerlach, G.; Krawietz, R.; Pompe, W.; Deineka, A.; Jastrabik, L. (2002), Characterization of RF-sputtered self-polarized PZT thin films for IR sensor arrays. *Vacuum* 66, 473

Sugiyama, O.; Kondo, Y.; Suzuki, H.; Kaneko, S. (2003), XPS Analysis of Lead Zirconate Titanate Thin Films Prepared Via Sol–Gel Process. *Journal of Sol–Gel Science and Technology*, 26, 749–52

Sugiyama, O.; Murakami, K.; Kaneko, S. (2004), XPS Analysis of Surface Layer of Sol–Gel-Derived PZT Thin Films, *Journal of European Ceramic Society*, 24, 1157–1160

Synowicki, A. (1998), Spectroscopic ellipsometry characterization of indium tin oxide film microstructure and optical constants. *Thin Solid Film,* 313 – 314, 394

Synowicki, R.A.; Tiwald, T. E. (2004), Optical properties of bulk c-ZrO_2, c-MgO and a-As_2S_3 determined by variable angle spectroscopic ellipsometry.*Thin Solid Film,* 455 – 456, 248

Tang, X. G.; Liu, Q. X.; Jiang L. L.; Ding, A.L. (2007), Optical properties of $Pb(Zr_xTi_{1-x})O_3$ (x= 0.4, 0.6) thin films on Pt-coated Si substrates studied by spectroscopic ellipsometry. *Materials Chemistry and Physics*, 103, 329

Tilley, D.R. (Gordon and Breach, Amsterdam, 1996), *Ferroelectric Thin Films*

Tompkins, H. G. Irene, E. A. (NY 2005), *Handbook of ellipsometry*

Trolier-McKinstry, S.; Koh, J. (1998), Composition profiling of graded dielectric function materials by spectroscopic ellipsometry. *Thin Solid Films,* 313-314, 389

Vidyarthi, V.S.; Lin, W.-M.; Suchaneck, G.; Gerlach, G.; Thiele, C.; Hoffmann, V. (2007), Plasma emission controlled multi-target reactive sputtering for in-situ crystallized $Pb(Zr,Ti)O_3$ thin films on 6" Si-wafers, *Thin Solid Films,* 515, 3547–3553

Wagner, C. (1971), Contribution to the thermodynamics of interstitial solid solutions. *Acta Metallurgica*, 19, 843-849

Wang, C. C.; Akbar, S. A. (1992), Decomposition of $YBa_2Cu_3O_x$ under an oxygen potential gradient using a YSZ-based galvanic cell. *Material Letters*, 13, 254–260

Wang, X.; Masumoto, H.; Someno, Y.; Chen, L.; Hirai., T. (2001), Stepwise graded refractive-index profiles for design of a narrow-bandpass filter. *Applied Optics,* 40, 3746

Wang, Y.G.; Zhong, W.L.; Zhang, P.L. (1995), Surface and size effects on ferroelectric films with domain structures. *Physical Review B*, 51, 5311

Watts, B. E.; Leccabue, F.; Fanciulli, M.; Ferrari, S.; Tallarida, G.; Parisoli, D. (2001), The influence of low temperature baking on the properties of $SrBi_2Ta_2O_9$ films from metallorganic solutions. *Integrated Ferroelectrics*, 37, 565–574.

Watts, B. E.; Leccabue, F.; Fanciulli, M.; Tallarida, G.; Ferrari, S. (2003), Surface segregation mechanisms in ferroelectric thin films. *Journal of Electroceramics*, 11, 139–147

Watts, B.E.; Leccabue, F.; Bocelli, G.; Padeletti, G.; Kaciulis, S.; Pandolfi, L. (2005), Lead enrichment at the surface of lead zirconate titanate thin films, *Journal of the European Ceramic Society,* 25, 2495–2498

Whatmore, R.W.; Zhang, Q.; Huang, Z.; Dorey, R.A. (2003), Ferroelectric thin and thick films for microsystems. *Materials Science in Semiconductor Processing*, 5, 65-76

Xi, J.-Q.; Schubert, M. F.; Kim, J. K.; Schubert, E. F.; Chen, M.; Lin, S.-Y.; Liu, W. ; Smart, J. A. (2007), Optical thin-film materials with low refractive index for broadband elimination of Fresnel reflection. *NaturePhotonics,* 1, 176

Yang, S.; Zhang Y.; Mo, D. (2006), A comparison of the optical properties of amorphous and polycrystalline PZT thin films deposited by the sol–gel method. *Materials Science and Engineering B,* 127, 117

Yee, Y.; Nam, H.-J.; Lee, S.-H.; Uk Bu, J.; Lee, J.-W. (2001), PZT actuated micromirror for fine-tracking mechanism of high-density optical data storage. *Sensors and Actuators A,* 89, 166-173

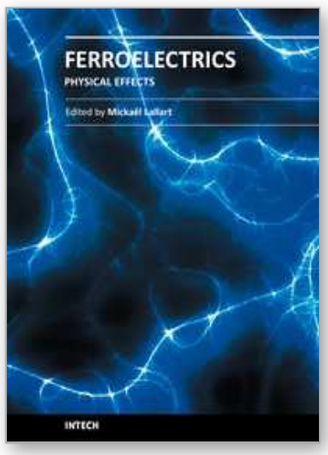

Ferroelectrics - Physical Effects

Edited by Dr. MickaÃ«l Lallart

ISBN 978-953-307-453-5
Hard cover, 654 pages
Publisher InTech
Published online 23, August, 2011
Published in print edition August, 2011

Ferroelectric materials have been and still are widely used in many applications, that have moved from sonar towards breakthrough technologies such as memories or optical devices. This book is a part of a four volume collection (covering material aspects, physical effects, characterization and modeling, and applications) and focuses on the underlying mechanisms of ferroelectric materials, including general ferroelectric effect, piezoelectricity, optical properties, and multiferroic and magnetoelectric devices. The aim of this book is to provide an up-to-date review of recent scientific findings and recent advances in the field of ferroelectric systems, allowing a deep understanding of the physical aspect of ferroelectricity.

InTech Europe
University Campus STeP Ri
Slavka Krautzeka 83/A
51000 Rijeka, Croatia
Phone: +385 (51) 770 447
Fax: +385 (51) 686 166
www.intechopen.com

InTech China
Unit 405, Office Block, Hotel Equatorial Shanghai
No.65, Yan An Road (West), Shanghai, 200040, China
中国上海市延安西路65号上海国际贵都大饭店办公楼405单元
Phone: +86-21-62489820
Fax: +86-21-62489821

IntechOpen